RSC Advances

ROYAL SOCIETY OF CHEMISTRY

www.rsc.org/advances

RSCAdvances RSCPublishing

ARTICLE

Adsorption of fluoride on Mg/Fe layered double hydroxides material prepared via hydrothermal process

Cite this: DOI: 10.1039/xoxxoooooox

Received ooth January XXXX,
Accepted ooth January XXXX

DOI: 10.1039/xoxxoooooox

www.rsc.org/

Tao Wu, [a] Lili Mao, [a] Haizeng Wang*[a]

ABSTRACT: A nitrate containing Mg/Fe layered double hydroxides (Mg/Fe-LDHs) material was prepared via hydrothermal process and the calcination product (Mg/Fe-LDHO) was used as adsorbent to remove fluoride from aqueous solution. Scanning electron microscopy (SEM), X-ray diffraction (XRD), Fourier transform-infrared spectroscopy (FT-IR), thermogravimetric analysis (TGA) and pHpzc analysis were used to characterize the samples. Inductively coupled plasma-atomic emission spectrometry (ICP-AES) was employed to analyse the dissolution of the metal ions from the synthesized adsorbent and commercial activated alumina respectively. Compared with commercial activated alumina, the synthesized adsorbent entirely avoided the potential risk of alumina and had a lower leakage of metal ions. A series of batch experiments were performed to investigate the effects of various experimental parameters, such as calcination temperature, adsorbent dosage, fluoride concentration, initial pH, contact time, adsorption temperature and co-existing anions. The results showed that 270℃was the optimal calcination temperature. The adsorption rapidly occurred in the initial 45min and adsorption equilibrium was established within 2.5h. Maximum desorption of 97.2% was achieved in the fluoride desorption studies at different pH. The adsorption data were well described by the pseudo-second-order kinetics model and the Langmuir isotherm model, and the adsorption capacity calculated by Langmuir equation was 28.65mg/g. In addition, the effects of co-existing anions on the adsorption capacity declined with the following order: PO_4^{3-}>CO_3^{2-} >SO_4^{2-} >NO_3^->Cl^-. It can be concluded that the synthetic adsorbent in this study is a promising material for fluoride removal from solutions.

1 Introduction

Appropriate ingestion of fluoride benefits human health, especially in inhibiting caries and helping tooth shell calcification. However, excess exposure to fluoride in drinking water can lead to harmful effects, such as dental/skeletal fluorosis [1]. The permissible maximum level of fluoride in drinking water set by World Health Organization (WHO) is 1.5 mg/L [2]. Unfortunately, fluoride pollution is a serious regional problem [3], especially in China, India, Pakistan, and Thailand [4]; millions of people in these countries are suffering from fluoride pollution. Thus it is of very importance to research how to remove fluoride from water with high fluoride concentration.

So far, various techniques have been developed to reduce the excess fluoride from water, including ion exchange [5], precipitation [6], electrodialysis [7] and adsorption [8]. Among the methods mentioned above, adsorption method attracts more attention because of its convenience, low cost and low-energy consumption [9-11]. Many adsorbents have been tested for the elimination of fluoride from water, such as activated alumina [12-13], activated carbons [14], aluminium alginate particles [15], organic-inorganic hybrid materials [16-17] and layered double hydroxides (LDHs) [18-22], and more. Compared with other materials, activated alumina was widely used for fluoride retention in China because it is economical and simple. Unfortunately, the unsatisfied adsorption capacity and high residual concentration of aluminium in the treated water are the insurmountable disadvantages for activated alumina. What is more, as we all know that aluminium exposure has proven to be a potential risk factor for the development or the speeding up of the Alzheimer syndrome [23]. In order to reduce aluminium content, W. Ma [24] used ferric ion to partly substitute aluminium and Mg/Al/Fe hydrotalcite-like compound was synthesized to remove fluoride, whereas, the removal efficiency was undesirable, and the problem of residual aluminium was not resolved absolutely. In recent years, a series of layered double hydroxides have been extensively studied as ion-exchangers and trapping agents for anionic contaminants because of their high capacity and affinity for a range of anions [19, 25]. It was found that the exchange between fluoride and nitrate ions occurred more easily than that between fluoride and carbonate ions [26]. And the anion exchange played an

important role during the adsorption process. Therefore, it was inferred that LDHs with nitrate ions as the interlayer anion would be better in the performance of fluoride adsorption than that of LDHs-CO_3^{2-}. It is worth to mention to the reader at this point that there is no published work that has used a Mg/Fe LDH for F^- removal.

In this paper, in order to increase the adsorption capacity and completely avoid the potential risk of alumina, nitrate containing Mg/Fe layered double hydroxides (Mg/Fe-LDHs) material was prepared via hydrothermal process, and was used to remove fluoride after being calcined. The resulting materials were characterized by SEM, XRD, FT-IR, TG, ICP-AES and pHpzc. Effective parameters such as calcination temperature, adsorbent dosage, fluoride concentration, initial pH, contact time, adsorption temperature and co-existing anions were investigated on fluoride removal. The adsorption isotherm and the adsorption kinetic of fluoride adsorption were also studied. Kinetic and isotherm studies were conducted to evaluate the adsorption capacity of the calcined product (Mg/Fe-LDHO).

2 Experimental

2.1 Materials

All reagents used in this study were analytical grade, and directly used without further purification. An appropriate volume of 0.1 mol/L HCl or NaOH solutions was used to adjust the pH of the solution. Deionized water was used throughout the synthesis and treatment processes.

2.2 Preparation of adsorbent

The nitrate containing Mg/Fe-LDHs with Mg^{2+}:Fe^{3+} molar ratio of 2:1 was prepared via hydrothermal process as detailed below. Alkaline solution (solution A) and mixed solution (solution B) containing $Mg(NO_3)_2 \cdot 6H_2O$ and $Fe(NO_3)_3 \cdot 9H_2O$ were respectively prepared with desired concentration. Then equivoluminal solution of A and B were simultaneously sucked into a beaker by peristaltic pumps at 25℃. Keep stirring and adjust the pump rate to keep the mixture at pH10-10.5[26]. After stirring for 1h, the precipitate formed was aged for 24h at 80℃ in reaction kettle, at end of which the precipitate was separated by filter. The wet cake was washed with deionized water until the pH of filtrate became neutral, and then was dried at 80℃ for 24 h to obtain Mg/Fe-LDHs. To triturate Mg/Fe-LDHs into powder and calcined at 270 ℃ for 3 h. The calcination product (Mg/Fe-LDHO) was used for the subsequent experiments.

2.3 Materials characterization

The surface morphology of the samples was observed by scanning electron microscope (SEM). The crystalline structure of the synthesized materials was determined by X-ray diffraction (XRD) employing a scanning rate 4˚/min in an angular range 2θ between 5 and 70˚ and Cu Kα as source of radiation. Fourier transform-infrared spectroscopy (FT-IR) was recorded in the range 4000-400 cm−1 and adopting the KBr tablet method. The element composition of the adsorbents was analysed by Inductively Coupled Plasma Atomic Emission Spectrometry (ICP-AES). The thermogravimetric analysis (TGA) was carried out by thermogravimetric analyser in nitrogen atmosphere under the heating rate of 10 ℃ per minute, varying from 25 to 800℃.

The pH at the point of zero charge (pHpzc) was determined using the pH drift method [27]. The pH of a solution of 0.01M NaCl was adjusted between 2 and 12 by adding either HCl or NaOH. Mg/Fe-LDHO (0.15g) was added to 50mL of the solution. The experiments were carried out in a thermostat shaker at 180 rpm and 25℃ for 24h. Then the suspensions were filtered and the final pH values were recorded. The results, plotted as final pH versus initial pH, yielded the PZC as the pH, at which initial pH and finial pH were equal.

2.4 Batch adsorption experiments

All the adsorption experiments were carried out in a temperature controlled shaker at 180 rpm with desired quantities of fluoride solution and adsorbent in conical flasks for a predetermined contact time, and then the suspensions were subjected to filtration. A selective electrode for fluoride ions [28] and ICP-AES was respectively used to measure the concentration of fluoride and ferric ions in the filtrate. In order to investigate the effect of initial pH on fluoride adsorption, the initial pH values were adjusted to 2-12 (adjusted with0.1 mol/L HCl and NaOH). The effect of contact time was collected at specific time intervals. To investigate the effect of co-existing anions on adsorption, moderate dosage of $NaNO_3$, NaCl, Na_2SO_4, Na_2CO_3 and Na_3PO_4 were respectively added to fluoride solutions. Adsorption isotherms were conducted at different temperature.

2.5 Desorption studies

The adsorbent that was used for the adsorption of fluoride was separated from solution (initial F concentration was 80mg/L) by filtration and dried at 80 ℃. Considering the dissolution of Mg/Fe-LDHO in acid solution, the pH 7-14 was selected for the desorption study. 0.2g adsorbent was agitated with 50mL of deionized water at different pH values for 2.5h, at 25℃. The concentration of desorption Fluoride was determined.

3 Results and discussion

3.1 Characterization of materials

SEM micrograph of the synthesized materials was depicted in Fig.1 (A, B, C) respectively. Fig.1 (A) shows that the adsorbent particle was stacked up by numerous nanosheets with a diameter of 100nm approximately. In addition, macroporous structure can be obviously observed. After calcination (Fig.1.B), the size of nanosheets and aperture was smaller than that aforementioned. The nanosheets became denser in arrangement and wizened on the morphology. This was caused by the loss of structural and adsorbed water during the calcination process. The nanosheets provided considerable superficial area for the later adsorption reaction, and the Nanoscale pores would serve as channel for solution diffusion. They provide favourable

condition for fluoride adsorption, which is proved by latish adsorption experiments.

From Fig.1(C), it was found that the morphology of the sample after adsorption was similar to the Mg/Fe-LDHs. Compared with Mg/Fe-LDHO; the nanosheets became more outstretched and the adsorbent particle had a looser stacking of nano-sheets. This can be explained

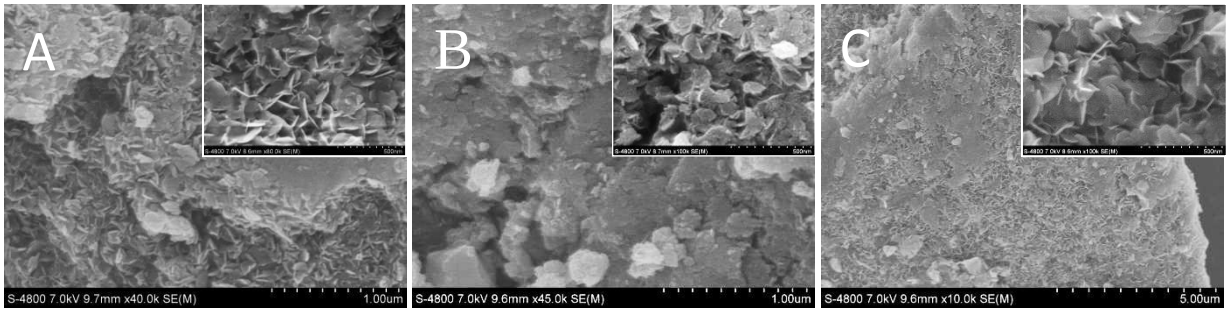

Fig.1 The SEM images of Mg/Fe-LDHs (A), Mg/Fe-LDHO (B) and Mg/Fe-LDHO after adsorption(C)

as following: Firstly, the solution of fluoride came into contact with nanosheets by penetrating into the aperture on the adsorbent particle, which leads to the expansion of the sheets. Secondly, during the adsorption process, the intercalation of fluoride and water molecule into the interlayer domain made the crystal structure reconstruct, which was in accordance with the X-ray results.

The XRD patterns of the samples and their calcined products were presented in Fig.2 (A). The indexed peaks (003, 006 and 009), as shown in Fig.2(A. c), were consistent with those observed in the literature for double layered hydroxides(LDHs) [29-32], which indicates that the synthesized product was double layered hydroxides. As is shown in Fig.2 (A. b), the characteristic peaks of LDHs disappeared after calcination at 270℃, which indicated the crystal structure was destroyed during the process. It was very interesting that the characteristic peaks reappeared to a certain extent after adsorption of fluoride, as shown in Fig.2 (A. a), which confirmed the reconstruction of crystal structure. That could be explained by the so called structure "memory effect" [33]. However, the decrease of peak intensity and the widening of diffraction line profile indicated that the crystallinity degree of the sample after adsorption was lower than that of Mg/Fe-LDHs.

The FTIR spectra of the samples are shown in Fig. 2 (B). The broad strong band observed around 3456.3 cm^{-1} was attributed to the overlap stretching vibrations of hydroxyl groups in the brucite-like layers, interlayer water and physically adsorbed water [34, 35]. The peak at 1651 cm^{-1} was due to bending mode of water molecules, which might be the evidence of the presence of water in the interlayer space. The strong absorption at 1382.9cm^{-1} was assigned to the ν_3 vibration of NO_3^-[35, 36, 37], which indicated the existence of interlamellar nitrate ions. All samples show bands around 572.8 cm^{-1} and 439.7 cm^{-1}, which were due to Mg-O and Fe-O lattice vibrations [38, 39]. In the case of calcined sample, as shown in Fig.2 (B. b), the intensity of peak at around 3456.3 cm^{-1} and 1651.0 cm^{-1} slightly decreased, which was caused by the evaporation of adsorbed and interlayer water, concomitant partial dehydroxylation of the brucite-like sheets. Compared with the FTIR spectrum of the calcined sample (curve b), remarkable changes were observed in that of Mg/Fe-LDHO after adsorption of fluoride (curve a). After adsorption of fluoride, the band at 1651 cm-1 is shifted to 1662.6 cm-1, which corroborated the interaction of fluoride with the hydroxyl groups. Furthermore, the intensity of peak attributed to the stretching vibrations of O-H and ν_3 vibration of NO_3^- significantly decreased, and a new sharp peak centred 3691.6 was observed after adsorption. The reason for the phenomenon mentioned above may be the removal of fluoride ions by replacing the hydroxyl ions and nitrate ions, which indicate that ion exchange played a role during the fluoride adsorption process.

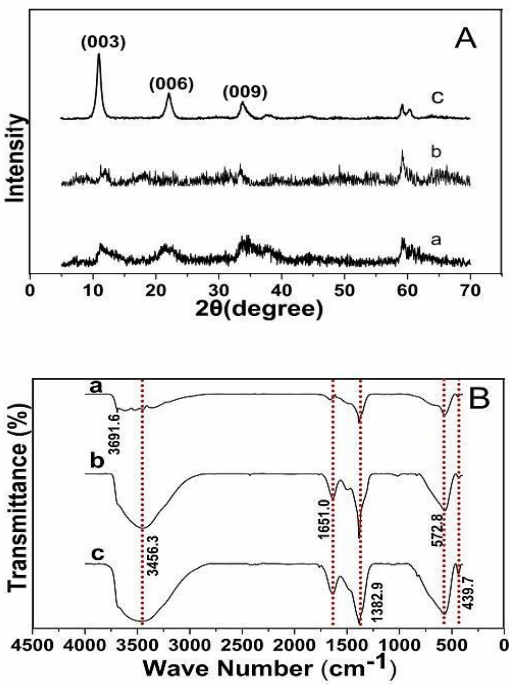

Fig.2 XRD (A) and FTIR (B) patterns of the samples, Mg/Fe-LDHs (a), Mg/Fe-LDHO (b), Mg/Fe-LDHO after adsorption (c)

The TGA curve of the synthesized Mg/Fe-LDHs was displayed in Fig.3 (a). The first (50-180℃, 13.59 mass%) weight-loss stage can be assigned to the evaporation of physically absorbed and interlayer water. Then, the sample

presented the dehydroxylation process of the brucite-like layers, between 180℃ and 345℃, corresponding to a mass loss of 14.41%. Another mass loss of 11.67% (345-600℃) can be ascribed to the decomposition of intercalated NO^{3-} anions. The TGA analysis provided a reference for the calcination in the succeeding experiment.

The pH_{PZC} of the adsorbent was approximate10.42 as shown in Fig.3 (b). The PZC value characterizes surface acidity: when oxide particles are introduced in an aqueous environment their surface charge is positive if pH (solution) <PZC and is negative if pH (solution) >PZC [25, 40]. Herein, the surface charge of Mg/Fe-LDHO adsorbent highly depends on the solution pH. When the solution pH is above 10.42, the surface of the adsorbent will have a net negative charge, while the adsorbent will have a positive charge when solution pH is below 10.42.

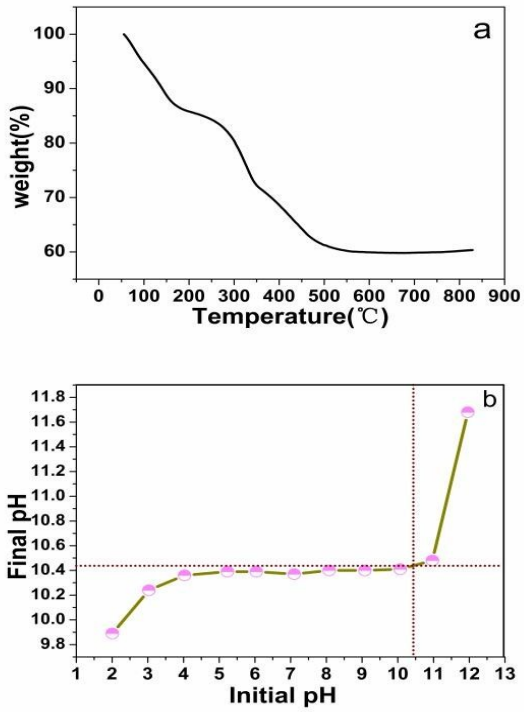

Fig.3 TGA (a) carve of Mg/Fe-LDHs and pH_{pzc} of Mg/Fe-LDHO (b)

The content analysis of Mg^{2+}, Fe^{3+} in Mg/Fe-LDHs was carried out by dissolving a certain amount of material in hydrochloric acid solution. ICP-AES was applied to determine the concentration of Mg^{2+} and Fe^{3+} ions. The ratio of Mg:Fe was found to be 2.056:1 compared to the theoretic ratio of 2:1. In addition, the stability of the synthesized adsorbent in fluoride solutions was determined and was compared with that of commercial activated alumina. Batch adsorption experiments of the synthesized adsorbent and commercial activated alumina were carried out in the same condition, and the liquid of adsorption equilibrium was subjected to ICP-AES analysis respectively. The result showed that the iron concentration was 0.0176mg/L, which was much lower than the standard of 0.3mg/L in drinking water set by the Ministry of Housing and Urban-Rural Development of the People's Republic of China (MOHURD). However, in comparison with the synthesized adsorbent, the leakage of alumina from commercial activated alumina was up to 2.726mg/L, which was much higher than the level of 0.2mg/L in drinking water set by the MOHURD. Herein, we can conclude that the synthesized adsorbent is more stable than commercial activated alumina in fluoride solution.

3.2 Adsorption behaviour of the synthetic adsorbent

3.2.1 Effect of calcination temperature. The fluoride adsorption capacity of Mg/Fe-LDHs calcined at various temperatures was investigated. As shown in Fig.4, the Mg/Fe-LDHs calcined at 270℃ achieved the maximum adsorption capacity of 16.91mg/g. Compared with the reported LDHs used as adsorbents , 270℃ was a lower calcination temperature relatively [41], which might relate to the insertion of nitrate ions. That may have a significant meaning for energy saving. Defluoridation from aqueous solution by layered double hydroxides usually occurs via three mechanisms [24]: (i) adsorption on external surface; (ii) intercalation by anion exchange; (iii) intercalation by reconstruction of calcined products (structure memory effect). Therefore, the maximum adsorption capacity would be achieved when the processes aforementioned simultaneously occurred. The "memory effect" may did not work if the LDHs were treated with lower temperature or exceeding calcination temperature. What's more, the exceeding calcination treatment may cause the collapse of pore structure which served as a channel for solution diffusion. In that case, the adsorption capacity will be severely affected. Hence, it is inferred that 270℃ is the optimal temperature for Mg/Fe-LDHs. At 270℃, the adsorbed and structural water were removed as much as possible, meanwhile, the pore structure and reestablishment of layered structure hardly be affected. This was in accordance with results of SEM and XRD. In terms of the results, Mg/Fe-LDHs calcined at 270℃ was selected to carry out the subsequent experiments.

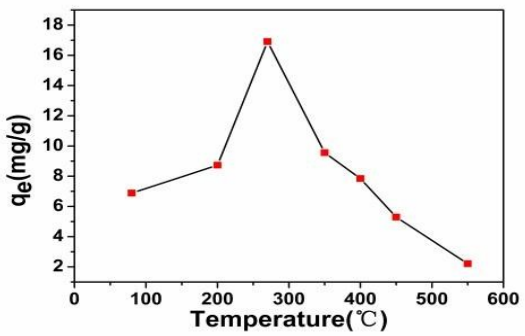

Fig.4 Effect of calcined temperature on the adsorption capacity (initial fluoride concentration 80mg/L; adsorbent dose 0.2g; 25℃)

3.2.2 Effect of adsorbent dosage and initial fluoride concentration. The effect of adsorbent dosage on the adsorption of fluoride with initial concentration of 80 mg/L was investigated and the results are shown in Fig.5. With the increase of adsorbent dosage, the adsorption capacity sharply decreased from 22.96mg/g to 12.64mg/g, while the removal efficiency significantly increased from 13.12% to 90.07%. The amount of fluoride in the solution and the adsorption sites on adsorbent of per unit weight was constant. With the increase of adsorbent dosage, there were more adsorptive sites to be employed for adsorption and more fluoride to be removed. However, with the increase of adsorbent dosage, a decrease of adsorption capacity was observed as a consequence of the

excess of adsorption sites which led to the decline in utilization efficiency of per unit weight adsorbent.

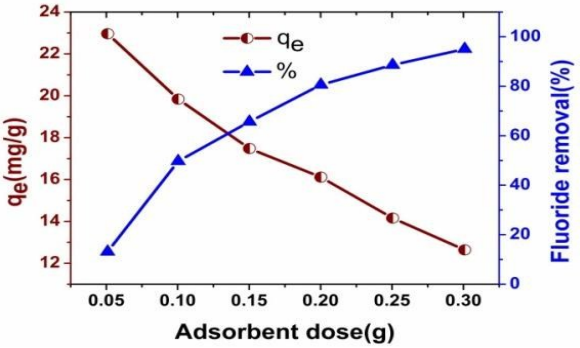

Fig.5 Effect of adsorbent dosage on the removal of fluoride (T=25℃, pH=7)

As shown in Fig. 6, with the initial fluoride concentration increasing from 10mg/L to 200mg/L, the adsorption capacity rose from 2.45mg/g to 25.88mg/g, which was accompanied with dramatic decline in fluoride removal efficiency. The minimum residual concentration of fluoride obtained is 1.41 mg/L with an initial of 30 mgF^-/L, which reaches the standard for drinking water quality. Higher initial fluoride concentration enhanced the driving force for fluoride to overcome the mass transfer resistance from liquid phases to the adsorbent particles [15]. The limited adsorption sites on the adsorbent particles were gradually occupied by fluoride with the increase of fluoride concentration. The decrease of defluorination efficiency can be explained by the fact that the ascendant rate of q_e is much lower than that of fluoride concentration. According to the results, adsorbent dosage (0.2g) and initial fluoride concentration (80mg/L) achieved high removal efficiency and adsorption capacity, thus we chosen adsorbent dosage of 0.2g and initial fluoride concentration of 80mg/L for the subsequent study.

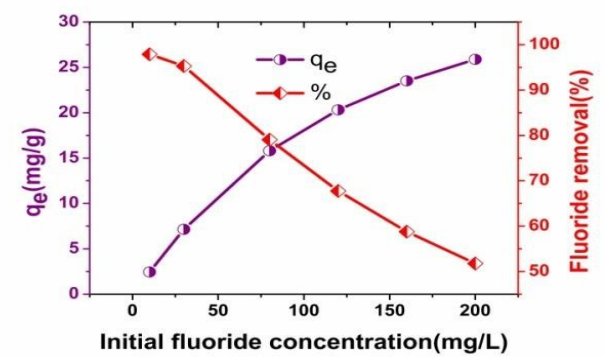

Fig.6 Effect of initial fluoride concentration on the removal of fluoride(T=25℃， pH=7)

3.2.3 Effect of initial pH and contact time. Fig.7 presents the fluoride adsorption on Me/Fe-LDHO over the initial pH range of 2-12. The adsorption capacity was almost constant at initial pH ranging from 2 to10, while a dramatically decrease was observed when the initial pH was above 10. The surface of the adsorbent was abundant in hydroxyl. As is mentioned before, the ion exchange between hydroxyl and fluoride played a role during the adsorption process, and there was a correlation between the exchange capacity and the net surface charge of the adsorbent. The adsorbent is cation exchanger in environments giving a negative surface charge and is anion exchanger in environments producing a positive surface charge [40]. Thus, the condition of pH below PZC of 10.42, at which the surface of the adsorbent had a net positive charge, was favourable for the removal of fluoride. Furthermore, the positive charge site on the adsorbent surface enhanced the adsorption of negatively charged fluoride through electrostatic forces attraction. At pH above PZC of 10.42, the surface of adsorbent became electronegative, and the electrical repulsion did not favour the fluoride uptake. In addition, the hydroxide concentration increased as pH is increased; this would compete with the fluoride for the adsorption sites [24]. Therefore, adsorption capacity significantly declined when the initial pH was above10.

The final pH of fluoride solution after adsorption was measured and presented in the graph (Fig.7). With the hydroxyl released from the adsorbent during the adsorption process, the pH of the solution increased. The two reactions[42] : $\equiv MOH + H_2O \Leftrightarrow \equiv MOH_2^+ + OH^-$ and $\equiv MOH + H_2O \Leftrightarrow \equiv MO\text{-}1 + H_3O^+$ where M indicates the metal element, would take place at acidic condition and basic condition respectively. It can be deduced that the adsorbent particles can buffer the fluctuation of pH in a certain range. Thus, the final pH stabilized around 9.30, while the initial pH was in the range of 4-10. According to the finial pH values of the solution, it was inferred that the effective pH range for fluoride removal was between 8 and 10 (i.e. at the initial pH 2-10). Given that a high adsorption was achieved near neutral initial pH. It was inferred that no pH adjustment was required in the treatment of drinking water with a neutral pH around 7. Therefore, the fluoride solution with initial pH=7 was used in the subsequent experiments.

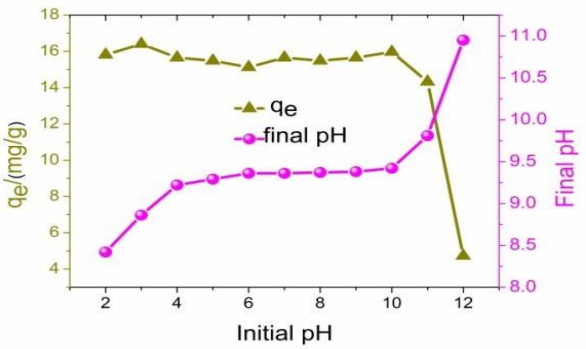

Fig.7 Effect of initial pH on the removal of fluoride (T=25℃)

Fig.8 displays the effect of contact time on fluoride adsorption. Obviously, in the initial 45min, the amount of fluoride adsorbed by Mg/Fe-LDHO increased rapidly, and then became slowly, finally reached equilibrium at about 2.5h. In the initial adsorption stage, the considerable amount of adsorption sites and fluoride enhanced the diffusion kinetics and the opportunities for fluoride adsorbed on the adsorbent. However, with the gradual occupancy of these adsorption sites and the decrease in fluoride concentration, the adsorption rate became more and more slowly until the equilibrium was finally reached. If the adsorption process was only controlled by an ion exchange mechanism, equilibrium time would be short. It suggested that the process of fluoride adsorption by Mg/Fe-LDHO was governed by complicated adsorption.

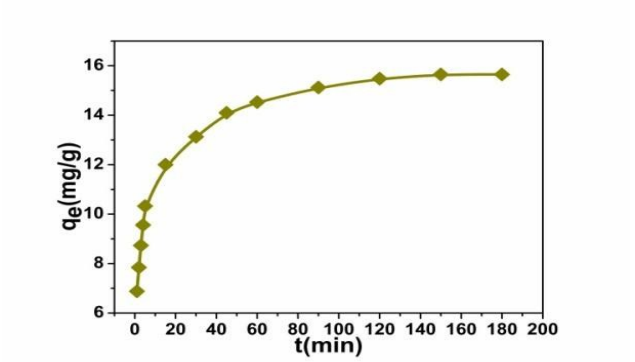

Fig.8 Effect of contact time on the removal of fluoride (T=25℃, pH=7)

3.2.4 Effect of adsorption temperature. The adsorption isotherms at different temperatures are shown in Fig.9. It was found that the influence of temperature on fluoride adsorption was almost negligible at lower equilibrium concentration (<17.4mg/L i.e., the initial concentration is lower than 80mg/L). However, an obvious decrease in adsorption capacity was observed when the equilibrium concentration was higher than 20mg/L (i.e., the initial concentration is higher than 80mg/L). The higher adsorption temperature was, the lower adsorption capacity would be. It indicates that the adsorption reaction was an exothermic reaction. At lower initial concentration, there were more vacant adsorptive sites, relative to fluoride, and the quantity of heat generated from adsorption reaction was insignificant to the solvent system. Hence, the nearly constant adsorption capacity for fluoride with lower initial concentration was observed, as shown in the graph. Once the concentration increased，adsorption reaction would produce more heat and be affected by temperature.

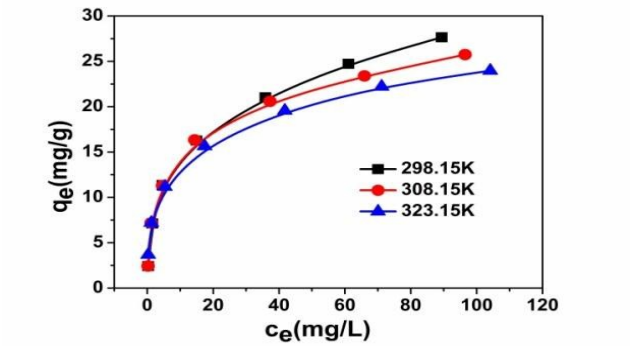

Fig.9 Effect of temperature on the removal of fluoride (pH=7)

3.2.5 Effect of co-existing anions. As a well-established knowledge that, the common ions such as Cl^- , NO_3^-, SO_4^{2-}, CO_3^{2-}, $PO_4^{3-}$are ubiquitous in drinking water or waste-waters. Thus, the competitive adsorption between the five diverse anions and fluoride were examined respectively. As depicted in Fig.10, the defluoridation performance exhibited negative trends in the presence of common anions. The most serious restraint on adsorption capacity came from PO_4^{3-} and was followed by CO_3^{2-}. The effect of Cl^- and NO_3^- was much weaker than that of PO_4^{3-} and CO_3^{2-}, then SO_4^{2-} was moderate .The effect of these anions on fluoride adsorption may be due to the electrostatic interaction between anions and adsorbent, which has greater affinities for anions with higher charge density [43,44]. Generally, multivalent anions were adsorbed more rapidly than monovalent anions [45]. The adsorption of co-existing anions leaded to the waste of limited adsorption sites on the adsorbent, which caused the decline in defluoridation capacity.

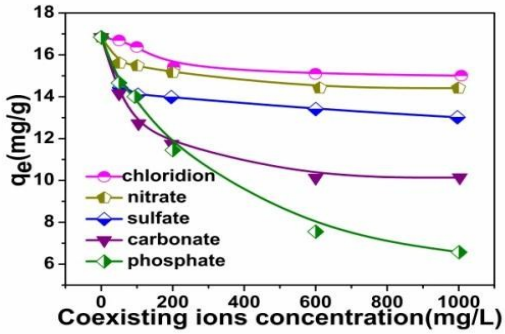

Fig.10 Effect of coexisting ions on removal efficiency of fluoride (T=25℃, pH=7)

3.3 Desorption studies

Desorption studies help to elucidate the mechanism and recovery of the adsorbent. As shown in Fig.11, desorption efficiency increased when the pH increased, and maximum fluoride releasing of 93.2% from the adsorbent was achieved in aqueous solution at pH 14. The pH condition which determined the electrical property of the adsorbent surface, would lead to the elimination of an ion present on the Mg/Fe-LDHO or, inversely, to the adsorption of an ion on the adsorbent. When the solution pH was above the PZC (10.42), the adsorbent surface would have a net negative charge, which favoured desorption of fluoride. In addition, with the increase of solution pH, the number of free hydroxide ion increased so that the adsorbed fluoride on the adsorbent surface was replaced. Because hydroxyl and fluoride have nearly the same size, they can exchange for each other [45].

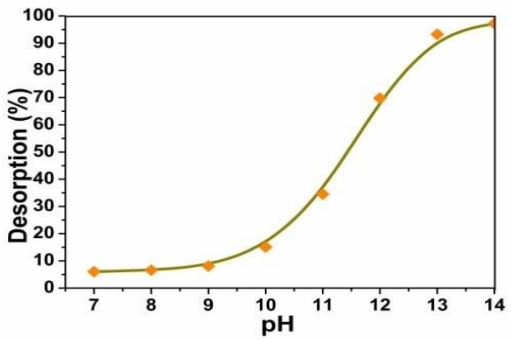

Fig.11 The effect of pH on desorption of fluoride

3.4 Adsorption isotherms

The adsorption isotherm indicates how the adsorbate interacts with adsorbents. It is basically important to describe how the adsorption molecules distribute between the liquid and the solid phase when the adsorption process reaches equilibrium, which will give some valuable information to optimize the design of new adsorption systems [46, 47]. Two-parameter models including Langmuir and Freundlich isotherms were widely used

to fit the experiment date. The Langmuir adsorption isotherm equation can be expressed as follows [48]:

$$\frac{C_e}{q_e} = \frac{1}{K_L q_m} + \frac{C_e}{q_m} \quad (3)$$

Where q_e and C_e are the equilibrium adsorption amounts (mg/g) and the equilibrium concentration of fluoride in solution (mg/L) respectively, q_m is the maximum fluoride adsorption capacity (mg/g), and K_L is the Langmuir constant which is related to the strength of adsorption. The Freundlich model can be described by the following equation [48].

$$\ln q_e = \ln K_f + \frac{1}{n} \ln C_e \quad (4)$$

Where K_f and $1/n$ are the constants related to the adsorption capacity and the adsorption intensity. The experimental dates for the isotherm modeling were the equilibrium data acquired from isothermal adsorption experiment at 298K.

The isotherm diagrams are presented in Fig.12 and the parameters obtained from the analysis of equilibrium data according to Langmuir and Freundlich linear model were listed in Table 1. The correlation coefficients (R^2) values of Langmuir model were higher than those of Freundlich model and the maximum adsorption capacity obtained from the Langmuir isotherm was very close to the experimental date, which implied the adsorption of fluoride onto the Mg/Fe-LDHs was more applicable for the Langmuir linear model. The result suggested that a monolayer adsorption played an important role in the adsorption process.

Table 1
The parameters of Langmuir and Freundlich isotherm models

T/K	Langmuir			Freundlich		
	q_m	K_L	R^2	K_f	n	R^2
298.15	28.645	0.135	0.984	5.016	2.465	0.957
308.15	26.108	0.172	0.990	5.451	2.712	0.946
323.15	24.510	0.170	0.990	6.122	3.227	0.981

3.4 Adsorption Kinetics

To express the mechanism of fluoride adsorption onto the surface of the adsorbent particles, the pseudo-first order rate model [49] and the pseudo-second order rate model [50] were used to analyse the present adsorption data obtained from experiment of contact time effect to determine the related kinetic parameters. The equations are expressed as follows:

$$\frac{dq_t}{dt} = K_1(q_e - q_t) \quad (5)$$

$$\frac{dq_t}{dt} = K_2(q_e - q_t)^2 \quad (6)$$

Where K_1 and K_2 are rate constants for the pseudo-first order (1/min) and the pseudo-second order adsorption (g/mg·min), respectively. While q_t and q_e are the amounts of fluoride adsorbed (mg/g) at time and at equilibrium, respectively.

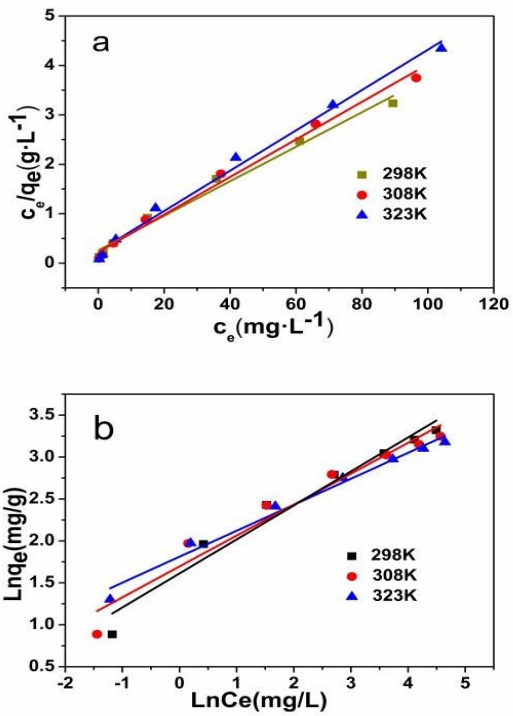

Fig.12 Adsorption isotherms of Langmuir (a) and Freundlich (b)

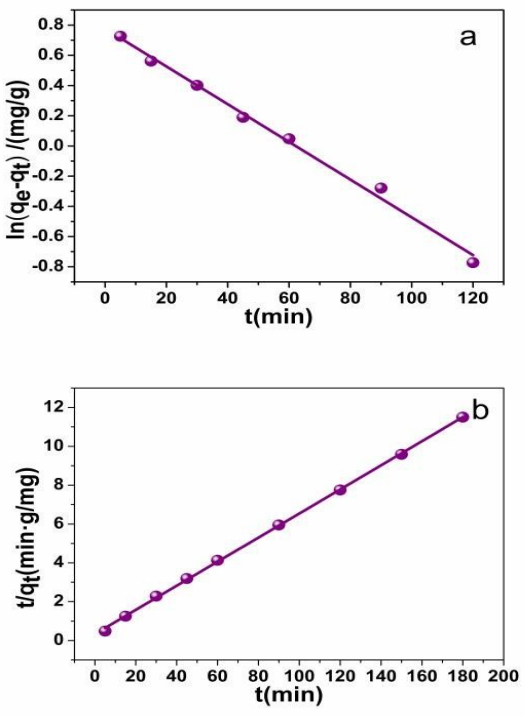

Fig.13 Kinetics adsorption models of pseudo first-order (a) and second-order (b)

Table 2
Adsorption kinetic parameters obtained by different models

$q_e$exp (mg/g)	Pseudo first-order			Pseudo second-order		
	q_e	K_1	R^2	q_e	K_2	R^2
15.65	5.98	0.029	0.993	16.12	0.012	0.999

The result was presented in Fig.13 and Table 2. As depicted in Table 2, the correlation coefficients (R^2) value of pseudo-second-order rate model was 0.999 which was higher than that of pseudo-first-order rate model (0.993). In addition, the adsorption capacity calculated by pseudo-second-order rate model was 16.12mg/g which was close to the experimental one (15.65mg/g). As discussed above, we can draw a conclusion that the adsorption kinetics date can be well described by the pseudo-second-order rate model.

4. Conclusions

A nitrate containing Mg/Fe-LDHs was successfully prepared for fluoride adsorption from aqueous solutions. After calcined at 270℃ for 3h, the Mg/Fe-LDHs showed excellent adsorption properties for fluoride at the pH 8-10. The residual fluoride was found to be 1.41mg/L with an initial concentration of 30mg/L, which meets the national standard for drinking water. The effects of co-existing anions on the adsorption capacity declined with the following order: $PO_4^{3-} > CO_3^{2-} > SO_4^{2-} > NO_3^- > Cl^-$. The kinetics adsorption experiment indicated that the adsorption equilibrium can be obtained within 2.5h. The adsorption date was well described by the Langmuir isotherm model and pseudo-second order kinetic model, and the adsorption capacity calculated by Langmuir equation was 28.65mg/g. Compared with the commercial activated alumina, the synthesized adsorbent with ignorable leakage of ferric ions completely avoided the potential risk of alumina. All of these indicate that the synthetic adsorbent is a promising material for fluoride removal from solutions.

Notes and references

[a] Kay Laboratory of Marine Chemistry Theory and Technology, Ministry of Education, College of Chemistry and Chemical Engineering, Ocean University of China, Qingdao, 266100, China
Email: haizwang@ouc.edu.cn; Wutoo2014 @126.com.
Tel: +86-532-66782503;

1 D. Fagin, *Sci. Am.*, 2008, **298**, 74-81.
2 World Health Organization (WHO), *World Health Organization, Geneva*, 2008, **1**, 185-186.
3 Q. Zhang, Q. Du, T. Jiao, Z. Zhang, S. Wang, Q. Sun and F. Gao, *Sci. Rep.*, 2013, **3**, 1-9.
4 L. Lv and X. Duan, *J. Hazard. Mater.*, 2006, **133**, 119-128.
5 F. Luo and K. Inoue, *Solvent Extra. Ion Exch.*, 2004, **22**, 305-322.
6 S. Saha, *Water Res.*, 1993, **27**, 1347-1350.
7 R.S. Keri, K.M. Hosamani, H.R.S. Reddy, S.K. Nataraj and T.M. Aminabhavi, *J. Water Chem. Technol.*, 2011, **33**, 293-300.
8 Q. Zhang, Q. Du, M. Hua, T. Jiao, F. Gao and B. Pan, *Environ. Sci. Technol.*, 2013, **47**, 6536-6544.
9 H. Deng and X. Yu, *Chem. Eng. J.*, 2012, **184**, 205-212.
10 Q. Chang, L. Zhu, Z. Luo, M. Lei, S. Zhang and H. Tang, *Ultrason. Sonochem.*, 2011, **18**, 553-561.
11 C.R.N. Rao and J. Karthikeyan, *Water Air Soil Poll.*, 2012, **223**, 1101-1114.
12 L.M. Camacho, A. Torres, D. Saha and S. Deng, *J. Colloid Interface Sci.*, 2010, **349**, 307-313.
13 S.S. Tripathy and A.M. Raichur, *Chem. Eng. J.*, 2008, **138**, 179-186.
14 A.A.M. Daifullah, S.M. Yakout and S.A. Elreefy, *J. Hazard. Mater.*, 2007, **147**, 633-643.
15 Q. Zhou, X. Lin, B. Li and X. Luo, *Chem. Eng. J.*, 2014, **256**, 306-315.
16 T. T. Moore and W. J. Koros, *Ind. Eng. Chem. Res.*, 2008, **47**, 591-598.
17 P. Koilraj and S. Kannan, *Chem. Eng. J.*, 2013, **234**, 406-415.
18 L. Lv, J. He, M. Wei, D.G. Evans and Z. Zhou, *Water Res.*, 2007, **41**, 1534-1542.
19 X. Zhao, L. Zhang, P. Xiong, W. Ma, N. Qian and W. Lu, *Micropor. Mesopor. Mat.*, 2015, **201**, 91-98.
20 S. Mandal and S. Mayadevi, *Appl. Clay Sci.*, 2008, **40**, 54-62.
21 P. Cai, H. Zheng, C. Wang, H. Ma, J. Hu, Y. Pu and P. Liang, *J. Hazard Mater.*, 2012, **213– 214**, 100– 108.
22 Y. Yu, L. Yu and J. P. Chen, *Chem. Eng. J.*, 2015, **l 262**, 839–846.
23 J. Das, B.S. Patra, N. Baliarsingh and K.M. Parida, *J. Colloid Interface Sci.*, 2007, **316**, 216-223.
24 W. Ma , N. Zhao, G. Yang, L. Tian and R. Wang, *Desalination*, 2011, **268**, 20-26.
25 I.M. Ahmed and M.S. Gasser, *Appl. Surf. Sci.*, 2012, **259**, 650– 656.
26 F. Cavani, F. Trifiro and A. Vaccari, *Catal. Today*, 1991, **11**, 173-301.
27 Y. F. Jia, B. Xiao and K.M. Thomas, *Langmuir*, 2002, **18**, 470-478.
28 C. D ńz-Nava, M. Solache-R ós and M.T. Olgu ń, *Sep. Sci. Technol.*, 2003, **38**, 131-147.
29 L. Batistella, L.D. Venquiaruto and M. D. Luccio, *Ind. Eng. Chem. Res.*, 2011, **50**, 6871-6876.
30 L. El Gaini, M. Lakraimi, E. Sebbar, A. Meghea and M. Bakasse, *J. Hazard Mater.*, 2009, **161**, 627-632.
31 M.A. Ulibarri, I. Pavlovic, C. Barriga, M.C. Hermos ń and J. Cornejo, *Appl. Clay Sci.*, 2001, **18**, 17-27.
32 M. Islam and R. Patel, *J. Hazard. Mater.*, 2009, **169**, 524-531.
33 F. Wong and R.G. Buchheit, *Prog. Org. Coat.*, 2004, **51**, 91–102.
34 M.A. Ulibarri, I. Pavlovic, C. Barriga and M.C. Hermos ń, *Appl. Clay Sci.*, 2001, **18**, 17-27.
35 F. P. d. S á, B. N. Cunha and L. M. Nunes, *Chem. Eng. J.*, 2013, **215–216**, 122–127.
36 J.T. Kloprogge, D. Wharton, L. Hickey and R.L. Frost, *Am. Mineral*, 2002, **87**, 623-629.
37 C. Li, G. Wang, D. V. Evans and X. Duan, *J. solid state chem.*, 2004, **177**, 4569-4575.
38 J. T. Kloprogge, L. Hickey and R. L. Frost, *Appl. Clay Sci.*, 2001, **18**, 37–49.
39 P, Huang, C. Cao, F. Wei, Y. Sun and W. Song, *RSC Adv.*, 2015, **5**, 10412-10417.
40 J.P. Reymond and F. Kolenda, *Powder Technol.*, 1999, **103**, 30–36.
41 W. Ma, T. Lv, X. Song, Z. Cheng, S. Duan, G. Xin, F. Liu and D. Pan, *J. Hazard. Mater.*, 2014, **268**, 166-176.
42 H. Wu, T. Wang, L. Chen and Y. Jin, *Ind. Eng. Chem. Res.*, 2009, **48**, 4530-4534.

43 L. Lv, J. He, M. Wei, D.G. Evans and X. Duan, *J. Hazard. Mater.*, 2006, **133**, 119–128.
44 D. Yang, Y. Li, Y. Wang and Z. Jiang, *RSC Adv.*, 2014, **4**, 49811-49818.
45 X. Zhao, J. Wang, F. Wu, T. Wang, Y. Cai, Y. Shi and G. Jiang, *J. Hazard. Mater.*, 2010, **173**, 102–109.
46 N.M. Mahmoodi, B. Hayati, M. Arami and C. Lan, *Desalination*, 2011, **268**, 117-125.
47 C.Y. Kuo, C.H. Wu and J.Y. Wu, *J. Colloid Interface Sci.*, 2008, **327**, 308-315.
48 X. Xu, Q. Li, H. Cui, J. Pang, L. Sun, H. An and J. Zhai, *Desalination*, 2011, **272**, 233-239.
49 Y.S. Ho and G. McKay, *Process Saf. Environ. Prot.*, 1998, **76**, 332–340.
50 Y.S. Ho and G. McKay, *Process Biochem.*, 1999, **34**, 451-465.